MOLECULAR METABOLISM

Fasting induces remodeling of the orexigenic projections from the arcuate nucleus to the hypothalamic paraventricular nucleus, in a growth hormone secretagogue receptor—dependent manner

Agustina Cabral [1,3], Gimena Fernandez [1,3], María J. Tolosa [1], Ángeles Rey Moggia [1], Gastón Calfa [2], Pablo N. De Francesco [1], Mario Perello [1,*]

ABSTRACT

Objective: Arcuate nucleus (ARC) neurons producing Agouti-related peptide (AgRP) and neuropeptide Y (NPY; ARC$^{AgRP/NPY}$ neurons) are activated under energy-deficit states. ARC$^{AgRP/NPY}$ neurons innervate the hypothalamic paraventricular nucleus (PVH), and ARC → PVH projections are recognized as key regulators of food intake. Plasma ghrelin levels increase under energy-deficit states and activate ARC$^{AgRP/NPY}$ neurons by acting on the growth hormone secretagogue receptor (GHSR). Here, we hypothesized that activation of ARC$^{AgRP/NPY}$ neurons in fasted mice would promote morphological remodeling of the ARC$^{AgRP/NPY}$ → PVH projections in a GHSR-dependent manner.

Methods: We performed 1) fluorescent immunohistochemistry, 2) imaging of green fluorescent protein (GFP) signal in NPY-GFP mice, and 3) DiI axonal labeling in brains of ad libitum fed or fasted mice with pharmacological or genetic blockage of the GHSR signaling and then estimated the density and strength of ARC$^{AgRP/NPY}$ → PVH fibers by assessing the mean fluorescence intensity, the absolute area with fluorescent signal, and the intensity of the fluorescent signal in the fluorescent area of the PVH.

Results: We found that 1) the density and strength of ARC$^{AgRP/NPY}$ fibers increase in the PVH of fasted mice, 2) the morphological remodeling of the ARC$^{AgRP/NPY}$ → PVH projections correlates with the activation of PVH neurons, and 3) PVH neurons are not activated in ARC-ablated mice. We also found that fasting-induced remodeling of ARC$^{AgRP/NPY}$ → PVH fibers and PVH activation are impaired in mice with pharmacological or genetic blockage of GHSR signaling.

Conclusion: This evidence shows that the connectivity between hypothalamic circuits controlling food intake can be remodeled in the adult brain, depending on the energy balance conditions, and that GHSR activity is a key regulator of this phenomenon.

1. INTRODUCTION

Based on his observations, Ramón y Cajal proposed early on that neurons in the adult brain are highly plastic cells and that their dendritic arbors and axonal collaterals can grow and retract under normal conditions [1]. Further studies not only confirmed this notion but also showed that morphological changes of neurons are functionally relevant [1]. Indeed, hypothalamic neurons are known to undergo a dramatic morphological remodeling that is critical to ensure the control of the body homeostasis [1]. For instance, morphological remodeling of

specific hypothalamic neurons occurs during dehydration, lactation, and through the ovarian cycle [2—4]. Some evidence also indicates that hypothalamic circuits controlling food intake show morphological and functional remodeling under energy-deficit conditions [5].

Neuronal populations of the hypothalamic arcuate nucleus (ARC) are key regulators of food intake. These populations include neurons that synthesize either Agouti-related peptide (AgRP) and neuropeptide Y (NPY) or pro-opiomelanocortin (POMC; hereafter named ARC$^{AgRP/NPY}$ and ARC^{POMC} neurons, respectively), which play opposing roles in energy balance: the activation of ARC$^{AgRP/NPY}$ neurons increases food

intake, while the activation of ARC[POMC] neurons inhibits it [6]. ARC neurons strongly innervate the hypothalamic paraventricular nucleus (PVH), and ARC→PVH projections are recognized as key regulators of food intake [7−10]. Under energy-deficit states, ARC[AgRP/NPY] neurons are activated [11]. The number of dendritic spines and the density of stimulatory synapses onto ARC[AgRP/NPY] neurons increase during fasting, and such an increase of the stimulatory transmission favors, in turn, ARC[AgRP/NPY] neuron activation [12]. This evidence suggests that ARC[AgRP/NPY] neurons can undergo morphological and functional remodeling that helps animals to cope with energy-deficit conditions. Here, we hypothesized that activation of ARC[AgRP/NPY] neurons in food-deprived mice would promote a morphological remodeling that would affect the density of their axonal fibers in the PVH.

Peripheral signaling systems control the activity of ARC[AgRP/NPY] neurons to adapt hypothalamic function to energy balance needs. The stomach-derived orexigenic hormone ghrelin plays a key regulatory role under energy-deficit states (i.e., fasting, calorie restriction), when plasma ghrelin levels increase [13,14]. Ghrelin promotes food-seeking behaviors and contributes to maintain glycemia [15,16]. The observation that mice lacking ghrelin display severe hypoglycemia and become moribund under food restriction strongly indicates that ghrelin plays essential functions to allow animal survival under energy-deficit states [15,17]. Ghrelin acts via the growth hormone secretagogue receptor (GHSR), which is particularly enriched in ARC[AgRP/NPY] neurons [18−24]. Ghrelin-induced food intake requires the presence of ARC[AgRP/NPY] neurons [21,25], and the expression of GHSR selectively in ARC[AgRP/NPY] neurons restores the gluco-regulatory effects of ghrelin observed upon caloric restriction [18]. Under fasting, GHSR gene expression also increases in ARC[AgRP/NPY] neurons, and ARC neurons become more sensitive to GHSR activation [11,26,27]. Notably, plasma ghrelin levels are similar in mice fasted for 12, 24, or 48 h, but hypothalamic GHSR mRNA levels as well as the sensitivity to ghrelin are higher in mice fasted for longer periods of time [28,29]. Thus, GHSR signaling in the brain seems to be more relevant when the energy deficit is more severe. Interestingly, GHSR protein remains elevated even several days after refeeding in mice previously fasted for 48 h, and such increment of GHSR level promotes the activation of ARC[AgRP/NPY] neurons and hyperphagia [30]. Thus, the upregulation of the GHSR activity in the hypothalamus is important not only during the fasting period to regulate metabolic adaptations to the energy deficit but also during the refeeding period to drive the behavioral changes required to reestablish the energy balance. Pharmacological blockage of ghrelin action reverses fasting-induced upregulation of excitatory synaptic inputs to ARC[AgRP/NPY], indicating that GHSR signaling under fasting also affects synaptic plasticity [31]. Because GHSR activity regulates long-term compensatory hyperphagia after a 48-h fasting event [30], we hypothesized that GHSR activity promotes a morphological remodeling of the ARC→PVH projections under severe fasting conditions.

Here, we compared ARC fibers in the PVH of adult mice fed ad libitum versus mice fasted for 48 h using complementary strategies: 1) fluorescent immunostaining against either AgRP or NPY, 2) imaging of the green fluorescent protein (GFP) signal in NPY-GFP mice, and 3) DiI axonal labeling. We found that the density and strength of ARC→PVH fibers are increased under fasting. To test whether these adaptations depended on GHSR signaling, we compared ARC→PVH fibers and the induction of the marker of neuronal activation c-Fos in the PVH of fasted mice either lacking GHSR expression or with pharmacological blockage of GHSR signaling.

2. MATERIALS AND METHODS

2.1. Animals

All studies were performed using 3- to 5-month-old male mice generated in the animal facility of the Multidisciplinary Institute of Cell Biology (IMBICE). Experimental mice included 1) wild-type (WT) mice, on a pure C57BL/6 background; 2) NPY-*Renilla* GFP (NPY-GFP) mice, in which the GFP is under the control of the NPY promoter (Jackson Laboratory, Stock #006417) [32]; 3) GHSR-deficient mice, which fail to express the GHSR [33] and were derived from crosses between heterozygous animals backcrossed 10 generations onto a C57BL/6 genetic background; 4) NPY-GFP/GHSR−deficient mice, which fail to express the GHSR and express the GFP under the control of the NPY promoter; and 5) ARC-ablated mice. To generate the ARC-ablated mice, 4-day-old pups were injected subcutaneously with either monosodium glutamate (2 mg/g body weight, Sigma-Aldrich, Cat# G1626) or 10% saline (ARC-intact mice), as described in a previous study [20]. Mice were housed under a controlled room temperature (22 ± 1 °C) and photoperiod (12-h light/dark cycle from 6:00 h to 18:00 h) with regular chow and water available ad libitum, except when indicated. Experiments were carried out in strict accordance with the recommendations in the Guide for the Care and Use of Laboratory Animals of the US National Research Council [34], and all efforts were made to minimize suffering. All protocols received approval from the Institutional Animal Care and Use Committee of the IMBICE (ID no. 10-0112).

2.2. Fasting protocol

Mice were single housed 3 days before starting the experiments, and fed ad libitum with regular chow. Individually housed mice were either fed ad libitum or fasted for 2 days, by removing the chow diet from the home cages at 10:00 h. In all cases, their body weight and food intake were manually monitored during the 2 days. Importantly, 2-day fasting is a manipulation fully tolerated by WT mice that display a normal overall health status and locomotor activity [29,30]. Experimental mice included 1) WT mice fed ad libitum (n = 4) or fasted (n = 4), NPY-GFP mice fed ad libitum (n = 5) or fasted (n = 5), GHSR-deficient mice fed ad libitum (n = 10) or fasted (n = 11) and their WT littermates fed ad libitum (n = 7) or fasted (n = 11), NPY-GFP/GHSR−deficient mice fed ad libitum (n = 6) or fasted (n = 5) and their NPY-GFP/WT littermates fed ad libitum (n = 5) or fasted (n = 5), and ARC-ablated mice fed ad libitum (n = 4) or fasted (n = 5) and ARC-intact mice fed ad libitum (n = 5) or fasted (n = 7). On the morning of the experimental day (between 9:00 h and 11:00 h), fed and fasted mice were anesthetized and perfused with formalin to obtain their brains.

2.3. DiI axonal labeling of ARC→PVH fibers

Individually housed mice were fed ad libitum (n = 4) or fasted for 2 days (n = 4) by removing their food at 10:00 h. On the morning of the experimental day, fed and fasted mice were deeply anesthetized with an intraperitoneal injection of chloral hydrate (500 mg/kg) and first transcardially perfused with ice-cold heparinized phosphate-buffered saline (PBS; 0.1 M, pH 7.4) and then fixed using ice-cold 4% paraformaldehyde (PFA; in 0.1 M PBS, pH 7.4). Brains were removed and post-fixed in the same fixative at 4 °C until further processing. For labeling, brains were sectioned from caudal to rostral to expose the ARC without disturbing the rostral regions. Next, brains were transferred and caudally glued to a chamber. Under a stereo-zoom microscope, each ARC was microinjected with a saturated solution of the dye 1,10-dioctadecyl-3,3,30,30-tetramethyl indocarbocyanine perchlorate (DiI, Invitrogen; Carlsbad, CA) in fish oil [35] using a patch

pipette and positive-pressure application [36,37]. Then, brains were stored in 4% PFA, and DiI was allowed to diffuse for 4 weeks in the dark at 37 °C. After DiI diffusion, brains were coronally cut in 40-μm-thick sections using a vibratome. Finally, brain sections containing the PVH were mounted onto glass slides and coverslipped with mounting media for posterior imaging analysis.

2.4. Fasting response in mice with pharmacological manipulations of the GHSR signaling

For intracerebroventricular (ICV) infusion, WT mice were first stereotaxically implanted with a single indwelling sterile guide cannula (Plastics One) into the lateral ventricle, with the following placement coordinates: anteroposterior, −0.34 mm; mediolateral, +1.00 mm; and dorsoventral, −2.30 mm, as previously described [38]. After surgery, mice were individually housed and allowed to recover for at least 5 days. During these days, mice were made accustomed to handling by removal of the dummy cannula and connection to an empty cannula connector. To block the GHSR signaling, WT mice were treated ICV with K-(D-1-Nal)-FwLL-NH$_2$ during the fasting period. K-(D-1-Nal)-FwLL-NH$_2$ was synthesized by automated solid-phase peptide synthesis as described elsewhere [39]. K-(D-1-Nal)-FwLL-NH$_2$ reduces ad libitum food intake in the early dark-phase period (from 18:00 h to 23:00 h), reduces ghrelin-induced 2-h food intake, and reduces fasting-induced hyperphagia exclusively in WT mice [30]. Here, fed and fasted mice were injected ICV with 2 μL of vehicle alone (artificial cerebrospinal fluid, n = 5 and n = 7, respectively) or containing K-(D-1-Nal)-FwLL-NH$_2$ (1 nmol/mouse, n = 4 and n = 7, respectively) every 8 h starting at 16:00 h of the first day of fasting and finishing at 8:00 h on the second day of fasting. Thus, each mouse received 6 ICV injections. The dose of K-(D-1-Nal)-FwLL-NH2 was chosen based on our previous study [30]. Mice were perfused around 10.00 h. In all cases, the correct placement of the cannula was confirmed by histological observation at the end of the experiment.

2.5. Immunohistochemistry

As previously described [40], brains of perfused mice were removed, post-fixed 2 h in fixative, immersed overnight in 20% sucrose, frozen, and coronally cut at 40 μm into four equal series on a sliding cryostat. One series of coronal sections was used for immunostaining. For fluorescent immunohistochemistry, brain sections were treated with blocking solution (3% normal donkey serum and 0.25% Triton X-100 in PBS) and incubated with the following antibodies: rabbit anti-NPY (1/7000; Abcam Cat# ab30914, RRID: AB_1566510), rabbit anti-AgRP (1/1000; Phoenix Pharmaceuticals Cat# H-003-57, RRID: AB_2313909), or rabbit anti-POMC (1/3000; Phoenix Pharmaceuticals Cat# H-029-30, RRID: AB_2307442) for 48 h at 4 °C. Then, sections were incubated with a donkey anti-rabbit Alexa Fluor 594 antibody (1/1000; Thermo Fisher Cat# A-21207, RRID: AB_141637) for 2 h. For chromogenic immunohistochemistry against c-Fos, sections were pretreated with 0.5% H$_2$O$_2$, treated with blocking solution (3% normal donkey serum and 0.25% Triton-X), and incubated with a rabbit anti−c-Fos antibody (1/3000; Santa Cruz Biotechnology Cat# sc7202, RRID: AB_2106765) for 48 h at 4 °C. Next, all sections were incubated with a biotinylated goat anti-rabbit antibody (1/3000; Vector Laboratories Cat# BA-1000, RRID: AB_2313606) for 1 h and then with the Vectastain Elite ABC (Vector Laboratories Cat# PK-6200) for 1 h, according to the manufacturer's protocols. Finally, a visible signal was developed with diaminobenzidine/nickel solution, resulting in a black/purple precipitate. Negative controls for immunostaining were also performed using the same procedure but omitting either the primary or secondary antibody. Sections were sequentially mounted on glass slides and coverslipped with mounting medium.

2.6. Validation of ARC-ablated mouse model

The ARC lesion was confirmed by ARC cell nuclei counting after thionin staining and AgRP immunostaining, described above. To visualize cell nuclei, brain sections were sequentially mounted on glass slides, washed with distilled H$_2$O, incubated with 0.025% thionin solution (Sigma-Aldrich, Cat# T7029), dehydrated in an ascending alcohol series, cleared in xylene, and coverslipped.

2.7. Quantitative neuroanatomical analysis

Bright-field color images were acquired with a Nikon Eclipse 50i and a DS-Ri1 Nikon digital camera with a 0.45 × adapter using a 10 ×/0.3 objective. All images were taken in comparable areas and under the same optical and light conditions. Fluorescence images were acquired with 10 ×/0.45, 20 ×/0.80, and a 63 ×/1.4 (oil) objectives using a Zeiss AxioObserver D1 equipped with an Apotome.2 structured illumination module and an AxioCam 506 monochrome camera. All image processing and analysis were performed in the ImageJ-based open-source image-processing package Fiji [41]. Fluorescent signal corresponding to AgRP+, NPY+, POMC+, and GFP+ was blindly and bilaterally quantified in the ARC and the PVH. For the ARC, the average fluorescence intensity within the nucleus was quantified in low-magnification (10 ×) images of one complete series of coronal sections per brain between bregma −0.70 and −0.94 mm [42]. For the PVH, fluorescent signal was quantified in high-magnification (63 ×) images centered in the compact part of the PVH, which was recognized beforehand by the distribution of cell nuclei labeled with Hoechst using low magnification, in one complete series of coronal sections per brain between bregma −1.58 and −1.94 mm [42]. For each image, the histogram of signal intensity was obtained, and the tissue background level was estimated by fitting a Gaussian curve, which coincided with the dominant peak. With these parameters, a specific signal detection threshold was calculated, which was defined as the mean of the distribution plus five standard deviations. A region of interest was created according to this threshold. In each image, three parameters were quantified: 1) the mean fluorescence intensity within this thresholded region, representing the average fluorescent signal per pixel; 2) the absolute area corresponding to this region, which represents the total number of pixels with significant levels of fluorescent signal in each image; and 3) the integrated density over this region, which represents the total the amount of significant fluorescent signal in the image. For quantification of the DiI+ fluorescent area in each PVH, a series of 18 adjacent optical sections were collected using a 20 ×/0.80 objective with a 0.95-μm z-axis interval in comparable areas under the same conditions. Then, the original z-stack was processed with the "Tubeness" Fiji plugin to enhance tubular features corresponding to the fibers. Maximum intensity projections for each series of processed images were prepared, log transformed, and then binarized according to histogram-based Gaussian-fit threshold parameters, as described above. For each binarized image, the fraction of area with fluorescent tubular structures within the PVH region (DiI+ area/PVH area) was obtained. The Fiji macros used for quantification are accessible at the Zenodo Repository (https://doi.org/10.5281/zenodo.3541615).

The number of c-Fos−positive (c-Fos+) cells in each brain region was quantified in one out of four complete series of coronal sections through the whole nuclei and was estimated per section. Blind quantitative analyses were performed independently by two observers. Neuroanatomical limits of the ARC and PVH were identified using a

Original Article

mouse brain atlas [42]. All data were corrected for double counting, according to the method of Abercrombie [43], in which the ratio of the actual number of neurons or cell nuclei to the observed number is represented by T/(T + h), where T = section thickness and h = the mean diameter of the cell nuclei along the z-axis. The mean diameter was determined using Fiji. To quantify c-Fos induction in ARC GFP+ cells, all GFP+ cells positive or negative for c-Fos were counted, and results were expressed as percentages representing GFP+ neurons positive for c-Fos compared with the total number of GFP+ cells observed.

2.8. Statistical analyses

Data were expressed as mean ± standard error of the mean (SEM). Equality of variance was analyzed using Bartlett's test. Unpaired *t* test with Welch correction was performed to compare fed and fasted data of WT and NPY-GFP mice. Two-way analysis of variance (ANOVA), followed by Tukey's post test, was used to compare data from fed and fasted conditions of WT- and GHSR-deficient, ARC-intact, and ARC-ablated, NPY-GFP/WT-deficient, and NPY-GFP/GHSR-deficient or vehicle and K-(D-1-Nal)-FwLL-NH$_2$ ICV-treated mice. Differences were considered significant when $p < 0.05$. Analyses were performed using GraphPad Prism, version 6.0 (GraphPad Software).

3. RESULTS

3.1. ARC$^{AgRP/NPY}$ → PVH fibers increase in fasted mice

The PVH is strongly regulated by the ARC, which senses peripheral signals and controls adaptations to the energy balance. Initially, we used fluorescent immunostaining to investigate whether ARC→PVH fibers are altered in fasted mice. We confirmed that NPY+ and AgRP+ fluorescence intensity increases 2.5 ± 0.1- and 2.7 ± 0.2-fold in the ARC of fasted mice, as compared with values found in fed mice ($p < 0.01$ in both cases; Figure 1A,F). To estimate the density and strength of ARC$^{AgRP/NPY}$→PVH fibers, we quantified three parameters: 1) the mean fluorescence intensity in the area corresponding to the PVH, which estimates the total amount of the neuropeptide in the PVH; 2) the absolute area with fluorescent signal, which estimates the density of fluorescent fibers in the PVH; and 3) the integrated density containing, which estimates the amount of fluorescent signal per fiber. In the PVH, NPY+ fluorescence intensity, NPY+ fluorescent area, and NPY+ integrated density increased in fasted mice (Figure 1B—E). Similarly, AgRP+ fluorescence intensity, AgRP+ fluorescent area, and AgRP+ integrated density increased in the PVH of fasted mice (Figure 1G—J). Notably, POMC + signal was 0.7 ± 0.1-fold smaller in the ARC of fasted mice compared with values found in fed mice ($p < 0.05$, Figure 1K), while POMC+ fluorescence intensity, POMC+ fluorescent area, and POMC+ integrated density in the PVH were unaffected in fasted mice (Figure 1L—O). Thus, the density and strength of the ARC$^{AgRP/NPY}$→PVH fibers increased in fasted mice. To assess whether such enhancement of ARC$^{AgRP/NPY}$→PVH fibers was associated with effects on neuronal activity, we assessed the number of c-Fos + cells in the ARC and PVH and found that it increased in both hypothalamic regions (3 ± 2 vs. 110 ± 8 and 3 ± 1 vs. 179 ± 15 c-Fos + cells/side/section in the ARC and PVH of fed and fasted mice, for both cases; see below). Thus, the increase in ARC$^{AgRP/NPY}$→PVH fibers correlates with an increase of c-Fos in the PVH.

A higher area with NPY+ and AgRP+ signal in the PVH of fasted mice could indicate either the presence of new fibers or the visualization of preexisting fibers that were not visualized in the fed condition because they lacked detectable levels of neuropeptides. To discriminate between these possibilities, we imaged the GFP+ fluorescent signal in the ARC and the PVH of NPY-GFP mice, in which GFP expression is under the control of the NPY promoter. The number of ARC GFP+ neurons did not differ between the fed and fasted NPY-GFP mice, suggesting that all ARC$^{AgRP/NPY}$ neurons are visualized in this mouse model, independently of the feeding condition (55 ± 8 vs. 63 ± 8 ARC GFP+ neurons/side/section in fed and fasted NPY-GFP mice, respectively; Figure 2A). Notably, the fluorescence intensity of ARC GFP+ cells increased 3.5 ± 0.3-fold in fasted mice as compared with that in fed mice ($p < 0.01$), suggesting that these neurons increased their transcriptional activity. In the PVH of NPY-GFP mice, not only GFP + fluorescence intensity and GFP+ integrated density signal but also the GFP+ fluorescent area increased in fasted mice (Figure 2B—E). In the ARC, the fraction of GFP+ neurons positive for c-Fos was significantly increased in fasted mice as compared with that in fed mice (2.3 ± 1.2 vs. 57.3 ± 6.5% for fed and fasted mice, respectively; Figure 2F—G).

As a complementary strategy to estimate if the density of ARC→PVH fibers changes in fasted mice, we performed an axonal labeling study in which we microinjected the lipophilic tracer DiI in the ARC of brains obtained from fed and fasted mice and then quantified the area corresponding to DiI+ fibers in the PVH (Figure 3A—B). In the PVH, the area of DiI+ fibers was significantly increased in fasted mice (Figure 3C). Of note, DiI+ fluorescence intensity and DiI+ integrated density were not estimated in this study because they have no biological meaning.

3.2. Fasting-induced activation of PVH neurons requires the ARC

Then, we tested whether the ARC is required for a fasting-induced activation of PVH neurons. Specifically, we assessed ARC$^{AgRP/NPY}$→PVH fibers and PVH activation in fasted ARC-ablated mice. ARC ablation was estimated using Nissl staining (Figure 4A—B), which confirmed that the number of cell bodies was reduced in the ARC of ARC-ablated mice as compared with ARC-intact mice (32 ± 6 vs.168 ± 6, $p < 0.001$), while it was not affected in the PVH (336 ± 16 vs. 319 ± 31). In terms of AgRP+ signal in the ARC, two-way ANOVA revealed no interaction but a main effect of both group, $F(1, 17) = 79.28$, $p < 0.001$, and condition, $F(1, 17) = 19.13$, $p < 0.001$, being increased in fasted ARC-intact mice but unaffected in ARC-ablated mice (Figure 4C,E). In terms of the AgRP+ signal in the PVH, two-way ANOVA revealed a significant interaction between group and condition for fluorescence intensity, $F(1, 17) = 5.75$, $p < 0.05$, fluorescent area, $F(1, 17) = 8.49$, $p < 0.01$, and integrated density, $F(1, 17) = 9.03$, $p < 0.01$. In particular, all these parameters were increased in fasted ARC-intact mice, while they were unaffected in ARC-ablated mice (Figure 4D,F—H). In terms of PVH activation, two-way ANOVA for the number of c-Fos+ cells revealed a significant interaction between group and condition in the ARC, $F(1, 12) = 91.12$, $p < 0.001$, and the PVH, $F(1, 12) = 93.54$, $p < 0.001$. In particular, the number of c-Fos+ cells increased in both the ARC and the PVH of fasted ARC-intact mice, while it was unaffected in ARC-ablated mice (Figure 5A—D).

3.3. Fasting-induced increase of ARC$^{AgRP/NPY}$ → PVH fibers and activation of PVH neurons requires GHSR signaling

Because ARC$^{AgRP/NPY}$ neurons are a key target of circulating ghrelin, whose concentration is increased in 48-h fasted mice [28,30], we hypothesized that GHSR signaling mediates these fasting-induced adaptations. Specifically, we investigated the ARC$^{AgRP/NPY}$→PVH fibers and the activation of PVH neurons in GHSR-deficient mice exposed, or not, to fasting. In terms of AgRP+ signal in the ARC, two-way ANOVA revealed a significant interaction between group and
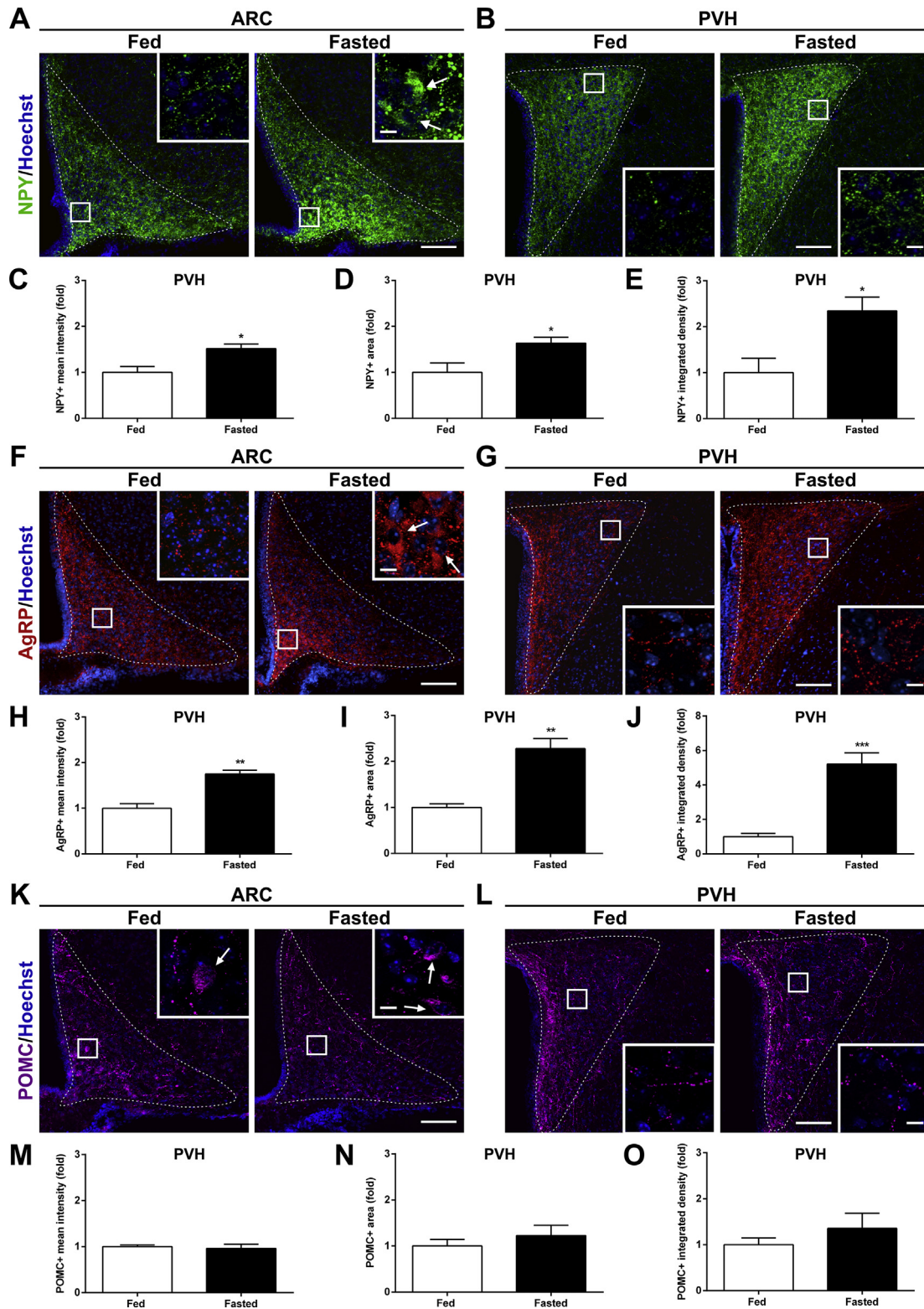
Figure 1: *ARC^AgRP/NPY → PVH projections increase in fasted WT mice.* **(A, B)** Representative photomicrographs of the ARC and PVH coronal sections of mice in each experimental group, respectively, subjected to immunofluorescence against NPY (Pseudo-colored to green), **(F, G)** AgRP (red), and **(K, L)** POMC (pseudo-colored to magenta). Insets in each image show high magnification of areas marked in low magnification images. Arrows point at positive cells. Scale bars: 100 μm (low magnification) and 10 μm (high magnification). Cell nuclei labeled with Hoechst (blue). **(C—E)** Bar graphs displaying the quantitative analysis of the mean fluorescence intensity, fluorescent area and integrated density of the NPY- (n = 4 per group), **(H—J)** AgRP- (n = 4 per group), and **(M—O)** POMC-positive signal (n = 4 per group) in the PVH of each experimental group. Data represent the mean ± SEM and were compared by unpaired t-test with Welch's correction. *p < 0.05, **p < 0.01 and ***p < 0.001 vs. fed condition.
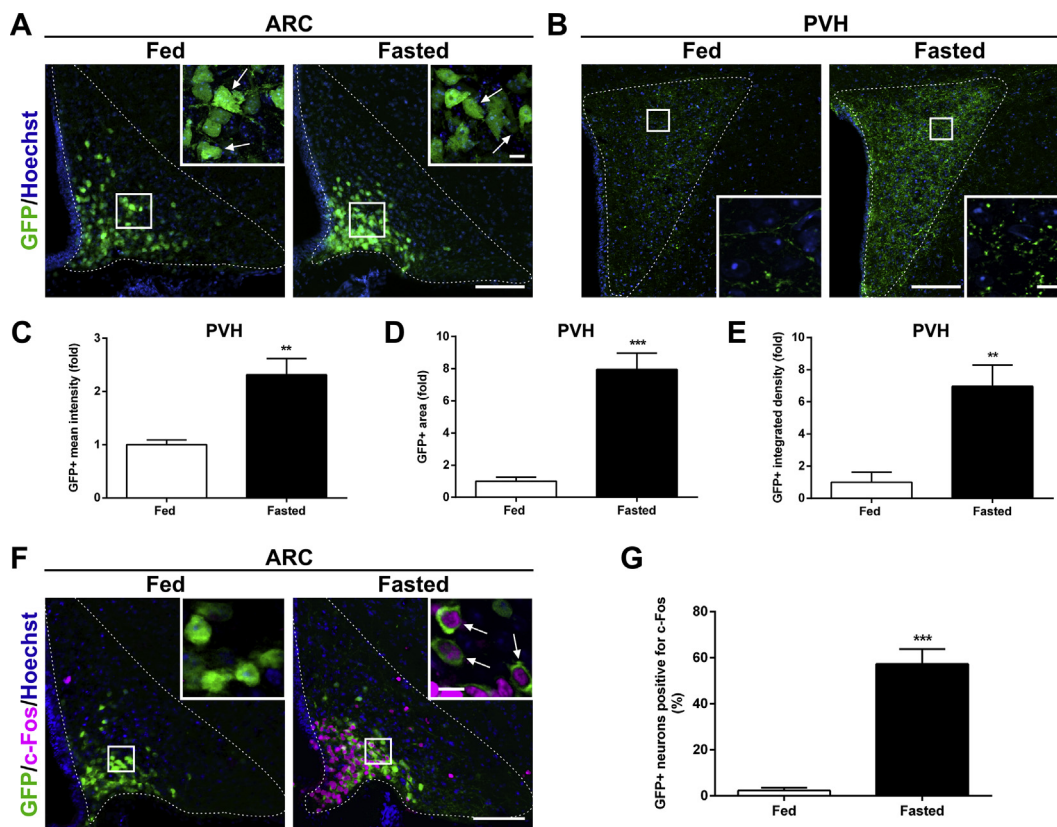
Figure 2: *ARC^NPY → PVH projections increase in fasted* NPY-GFP *mice.* **(A, B)** Representative photomicrographs showing the ARC and PVH coronal sections of NPY-GFP mice in each experimental group, respectively. Insets in each image show high magnification of areas marked in low magnification images. Arrows point at GFP-positive cells. Scale bars: 100 μm (low magnification) and 10 μm (high magnification). **(C−E)** Bar graphs displaying the quantitative analysis of the mean fluorescence intensity, fluorescent area and integrated density of the GFP-positive signal in the PVH of each experimental group (n = 5 per group). **(F)** Representative photomicrographs of the ARC coronal sections of NPY-GFP mice in each experimental group subjected to chromogenic immunostaining against c-Fos (Pseudo-colored to magenta). Insets in each image show high magnification of areas marked in low magnification images. Arrows point at dual-labeled cells. Scale bars: 100 μm (low magnification) and 10 μm (high magnification). Cell nuclei labeled with Hoechst (blue). **(G)** Bar graph displaying the percentage of GFP+ cells positive for c-Fos in the ARC in each experimental condition (n = 4 and n = 6 for fed and fasted group, respectively). Data represent the mean ± SEM and were compared by unpaired t-test with Welch's correction. **p < 0.01 and ***p < 0.001 vs. fed condition.

condition, $F_{(1, 13)} = 13.36$, $p < 0.01$, being increased in fasted WT mice but unaffected in GHSR-deficient mice (Figure 6A,C). In terms of AgRP+ signal in the PVH, two-way ANOVA for the AgRP+ signal revealed a significant interaction between group and condition for fluorescence intensity, $F_{(1, 13)} = 4.67$, $p < 0.05$; fluorescent area, $F_{(1, 13)} = 10.52$, $p < 0.01$; and integrated density, $F_{(1, 13)} = 17.12$, $p < 0.01$. In particular, all these parameters were increased in fed GHSR-deficient mice as compared with fed WT mice and were not affected by fasting (Figure 6B, D−F). In terms of the number of c-Fos+ cells, two-way ANOVA revealed a significant interaction between group and condition in the ARC, $F_{(1, 35)} = 27.78$, $p < 0.001$, and the PVH, $F_{(1, 35)} = 59.63$, $p < 0.001$. In the ARC, the number of c-Fos+ cells increased in both fasted experimental groups, but the increment was significantly smaller in GHSR-deficient mice as compared with WT mice (Figure 6G and Supplementary Fig. 1). In the PVH, the number of c-Fos + cells increased in fasted WT mice as compared to that in fed WT mice and remained unchanged in fasted GHSR-deficient mice as compared with fed GHSR-deficient mice (Figure 6H, and Supplementary Fig. 1).

We also assessed the GFP+ signal in the ARC and the PVH of NPY-GFP/GHSR−deficient mice. In terms of the GFP+ signal in the ARC, the number of ARC GFP+ neurons did not differ between fed and fasted NPY-GFP/GHSR−deficient mice, as seen in NPY-GFP/WT mice (not

shown, Figure 7A). However, two-way ANOVA revealed a significant interaction between group and condition for GFP+ intensity, $F_{(1, 17)} = 11.30$, $p < 0.01$, being increased in fasted NPY-GFP/WT mice but unaffected in NPY-GFP/GHSR−deficient mice (Figure 7A,C). In terms of GFP + signal in the PVH, two-way ANOVA revealed a significant interaction between group and condition for fluorescence intensity, $F_{(1, 17)} = 15.23$, $p < 0.01$; fluorescent area, $F_{(1, 17)} = 5.94$, $p < 0.05$; and integrated density, $F_{(1, 17)} = 8.62$, $p < 0.01$. In particular, all these parameters were increased in fed NPY-GFP/GHSR−deficient mice as compared with fed NPY-GFP/WT mice and were not affected by fasting (Figure 7B, D−F).

Because GHSR-deficient mice displayed higher ARC^AgRP/NPY → PVH fibers in the fed condition, it is unclear if the lack of fasting-induced effects on these fibers was due to the absence of the GHSR signaling or an inability of the ARC^AgRP/NPY → PVH fibers to be upregulated above their basal levels. Thus, we used a pharmacological approach to test if GHSR signaling is required for the fasting-induced increase of the density of ARC^AgRP/NPY → PVH fibers and activation of PVH. Specifically, we investigated the ARC^AgRP/NPY → PVH fibers and the level of PVH activation in fasted WT mice injected ICV with the GHSR blocker K-(D-1-Nal)-FwLL-NH$_2$. In a similar fashion, as we already showed for NPY+ signal in the ARC [30], two-way ANOVA for AgRP+ signal in the ARC revealed a significant interaction between
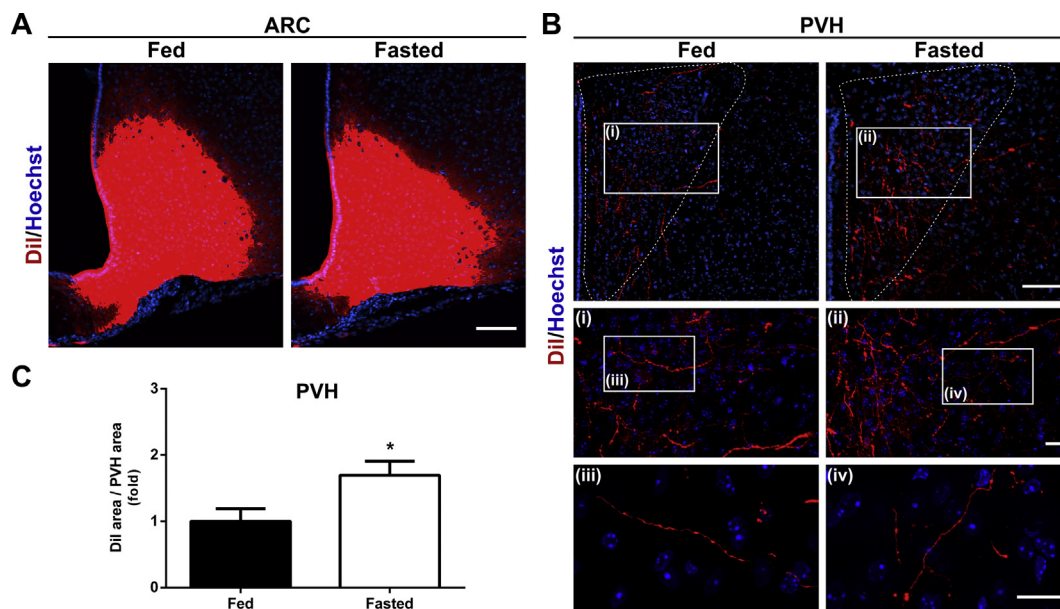
Figure 3: *ARC→PVH projections increase in fasted mice.* **(A)** Representative photomicrographs showing the localization of the DiI labeling in the ARC of mice in each experimental group. Scale bar: 100 µm. **(B)** Low magnification photomicrographs showing the ARC DiI-labeled fibers in the PVH of mice in each experimental group. Insets in each image depict high magnification images of the areas marked in low magnification images. Scale bars: 100 µm (low magnification) and 50 µm (high magnification). Cell nuclei labeled with Hoechst (blue). **(C)** Bar graph displaying the quantitative analysis of the area of DiI-labeled fibers in the PVH of mice in each experimental group (n = 8 per group). Data represent the mean ± SEM and were compared by unpaired t-test with Welch's correction. *p < 0.05 vs. fed condition.

group and condition, $F(1, 12) = 12.00$, $p < 0.01$, with the AgRP+ signal being increased in fasted mice treated ICV with vehicle, while it was unaffected in fasted mice treated ICV with K-(D-1-Nal)-FwLL-NH$_2$ (Figure 8A,C). In terms of AgRP+ signal in the PVH, two-way ANOVA for AgRP + signal revealed a significant interaction between group and condition for fluorescence intensity, $F(1, 12) = 17.17$, $p < 0.01$; fluorescent area, $F(1, 12) = 15.93$, $p < 0.01$; and integrated density, $F(1, 12) = 33.01$, $p < 0.001$. In particular, all these parameters were increased in fasted mice treated ICV with vehicle, while they were unaffected in fasted mice treated ICV with K-(D-1-Nal)-FwLL-NH$_2$ (Figure 8B, D−F). In line with these observations, two-way ANOVA for the number of c-Fos+ cells revealed a significant interaction between group and condition in the ARC, $F(1, 19) = 11.62$, $p < 0.01$, and the PVH, $F(1, 19) = 29.22$, $p < 0.001$. In particular, the number of c-Fos+ cells increased in both the ARC and the PVH of both fasted experimental groups, but the increment was significantly smaller in fasted mice treated ICV with K-(D-1-Nal)-FwLL-NH$_2$ as compared to that in fasted mice treated ICV with vehicle (Figure 8G−H; Supplementary Fig. 2).

4. DISCUSSION

There are two main findings in this study. First, ARC$^{AgRP/NPY}$→PVH fibers undergo to dramatic morphological remodeling under fasting. In particular, we found that the density and strength of ARC$^{AgRP/NPY}$→PVH fibers increase in fasted mice. We also found that the morphological remodeling of the ARC$^{AgRP/NPY}$→PVH fibers correlates with the activation of PVH neurons and that PVH neurons are not activated in ARC-ablated mice. Thus, the fasting-induced remodeling of the ARC$^{AgRP/NPY}$→PVH fibers seems to affect the activity of the PVH. Second, we found that the remodeling and PVH activation of fasting-induced ARC$^{AgRP/NPY}$→PVH fibers is impaired in mice either lacking GHSR expression or with pharmacological blockage of GHSR signaling.

To our knowledge, this is the first evidence that the ARC→PVH fibers can be remodeled in the adult brain, depending on the energy balance conditions, and that GHSR activity is a key regulator of this phenomenon.

Under fasting conditions, ARC$^{AgRP/NPY}$ neurons are activated and ARC^{POMC} neurons are inhibited [7,31,44−46]. The mechanism controlling the activation of ARC$^{AgRP/NPY}$ neurons in fasting is controversial because initial studies showed that it depends on intrinsic changes of neuronal electrical activity, independently of synaptic inputs [45,47], while further studies reported that it requires an increase in the number of dendritic spines and the density of stimulatory synapses onto ARC$^{AgRP/NPY}$ neurons [12]. Fasting-induced inhibition of ARC^{POMC} neurons is partially mediated by activation of ARC$^{AgRP/NPY}$ neurons [48,49]. ARC neurons strongly innervate the PVH, which coordinates a variety of neuroendocrine, autonomic, and behavioral responses [21,50−52]. To estimate whether ARC→PVH projections change under fasting, we used three complementary strategies. First, we performed immunostaining against AgRP and NPY. AgRP is exclusively produced in the ARC [53,54], while NPY is also produced in other brain areas, but NPY+ fibers in the PVH are mainly derived from the ARC [55]. Imaging of the AgRP+ and NPY+ signals in the PVH indicated that the density of ARC$^{AgRP/NPY}$→PVH fibers and the amount of orexigenic neuropeptides per fiber increase under fasting. Immunostaining against POMC confirmed that biosynthesis of anorexigenic POMC-derived peptides in the ARC is reduced under fasting [30,46,56]; however, we found that the POMC+ signal in the PVH is unaltered under this condition. The lack of decrease of POMC+ signal in the PVH under fasting may result from the accumulation of POMC-derived peptides in ARC^{POMC}→PVH projections, since the secretion of these neuropeptides is reduced under fasting [57,58]. Imaging analysis of the GFP+ signal in the PVH of NPY-GFP mice also showed that the density and strength of ARC^{NPY}→PVH fibers increase under fasting. In addition, axonal labeling studies confirmed that the density
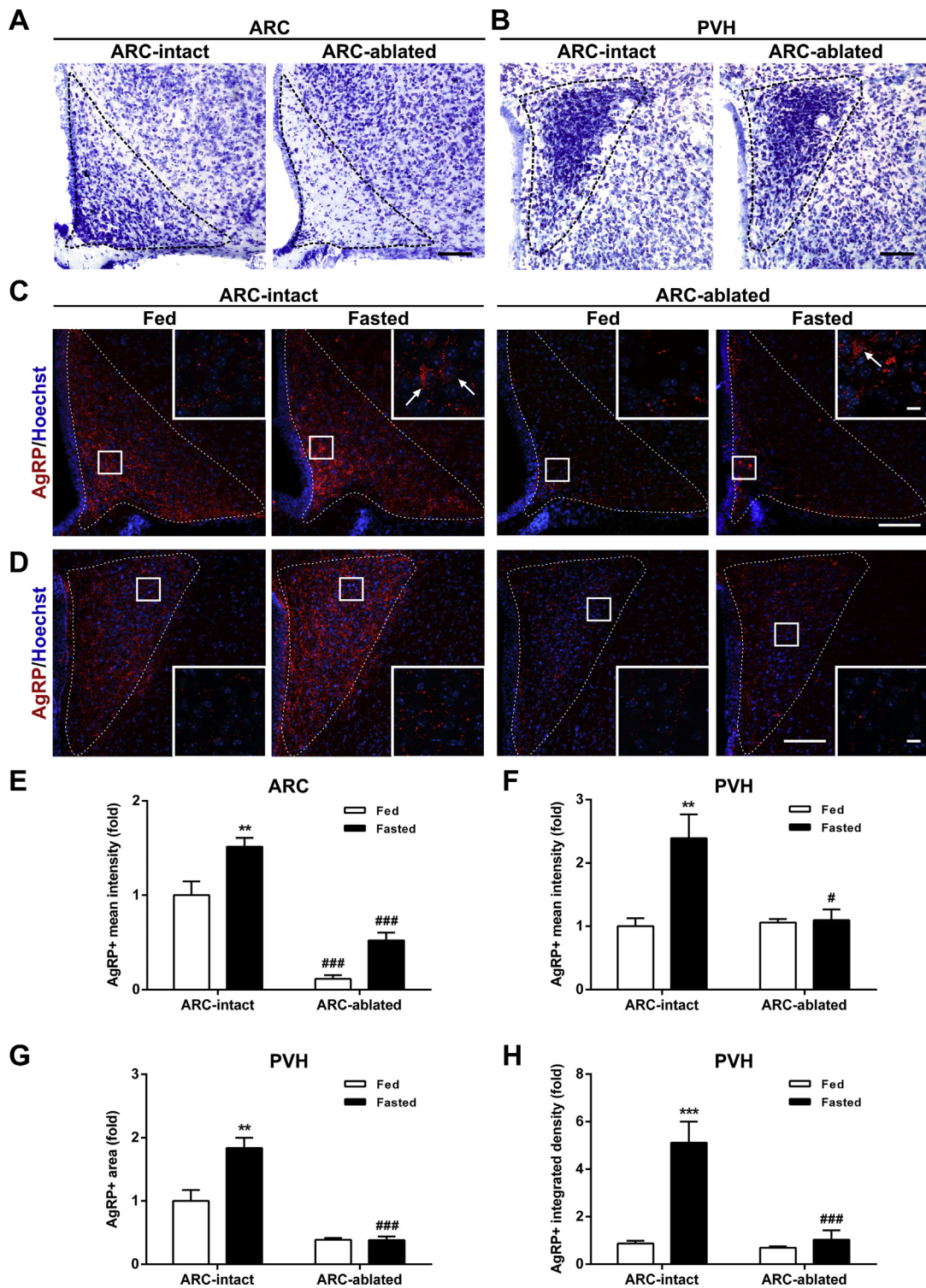
Figure 4: *Fasting-induced increase in ARC$^{AgRP/NPY}$ → PVH projections is impaired in ARC-ablated mice.* **(A, B)** Representative photomicrographs of Nissl staining of the ARC and PVH, respectively, of ARC-intact and ARC-ablated mice. Scale bar: 100 μm. **(C, D)** Representative photomicrographs of the ARC and PVH coronal sections, respectively, of ARC-intact and ARC-ablated mice in each experimental group, subjected to immunofluorescence against AgRP (red). Insets in each image depict high magnification images of the areas marked in low magnification images. Arrows point at AgRP-positive cells. Scale bars: 100 μm (low magnification) and 10 μm (high magnification). Cell nuclei labeled with Hoechst (blue). **(E)** Bar graph displaying the quantitative analysis of the mean fluorescence intensity of the AgRP-positive signal in the ARC of each experimental group (n = 4–7). **(F–H)** Bar graphs displaying the quantitative analysis of the mean fluorescence intensity, fluorescent area and integrated density of the AgRP-positive signal in the PVH of each experimental group (n = 4–7). Data represent the mean ± SEM and were compared by two-way ANOVA. **p < 0.01 and ***p < 0.001 vs. different condition, same group; #p < 0.05 and ###p < 0.001 vs. same condition, different group.
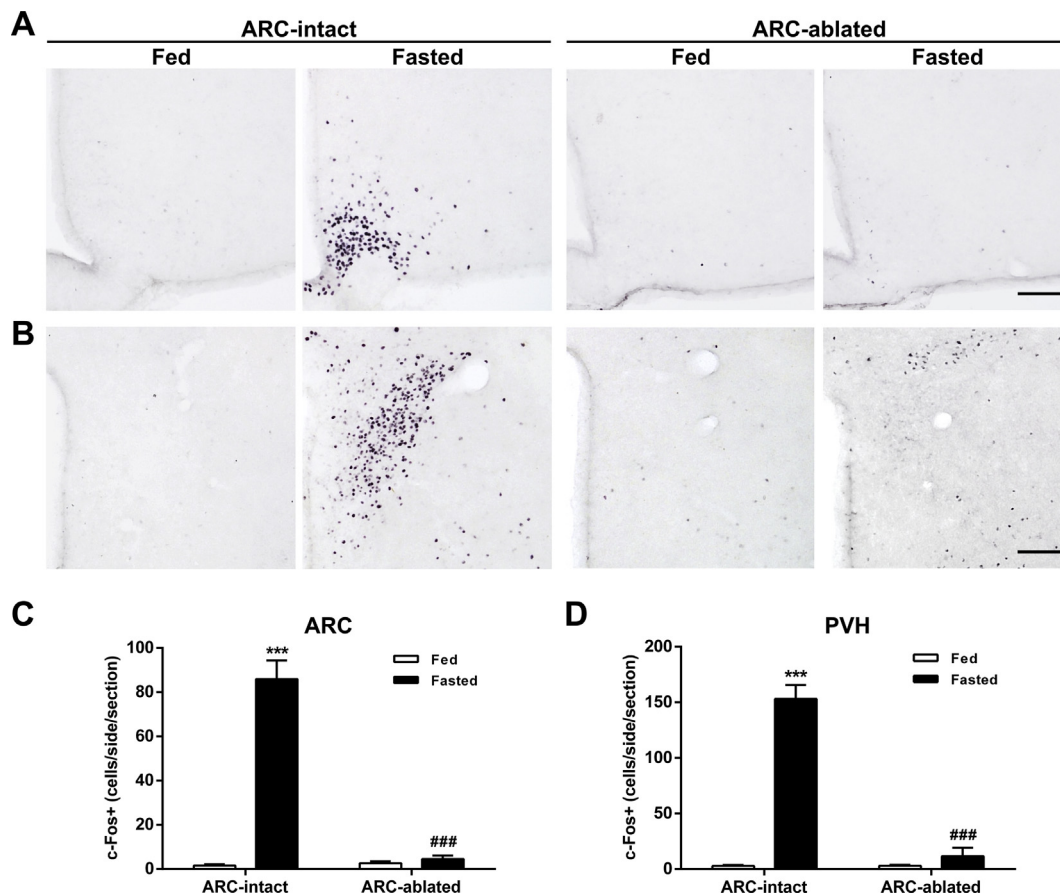
Figure 5: *Fasting-induced increase of c-Fos levels in the PVH is impaired in ARC-ablated mice.* **(A, B)** Representative photomicrographs of the ARC and PVH coronal sections, respectively, of ARC-intact and ARC-ablated mice in each experimental group, subjected to chromogenic immunostaining against c-Fos. **(C, D)** Bar graphs displaying the quantitative analysis of the number of c-Fos-positive cells in the ARC and PVH, respectively, of each experimental group (n = 4). Data represent the mean ± SEM and were compared by two-way ANOVA. ***$p < 0.001$ vs. different condition, same group; ###$p < 0.001$ vs. same condition, different group.

of ARC→PVH fibers increases under fasting. In this case, the DiI + signal does not allow for the discrimination of the identity of the ARC→PVH fibers; however, immunostaining analysis and imaging analysis in the NPY-GFP mice strongly support the notion that ARC$^{AgRP/NPY}$→PVH fibers are one of the main contributors to this observation. Notably, the increment of the density and strength of ARC$^{AgRP/NPY}$→PVH fibers correlates with an activation of the PVH neurons, and fasting-induced activation of PVH neurons is impaired in ARC-ablated mice, in which ARC$^{AgRP/NPY}$→PVH fibers are not affected under fasting. Thus, the density and strength of ARC$^{AgRP/NPY}$→PVH projections are enhanced under fasting, and such remodeling seems to play a key role in the activation of the PVH. In line with the possibility that ARC→PVH projections remain plastic in the adult brain, a recent study showed that the reactivation of the leptin receptor expression in adult mice increases the density of ARC→PVH fibers as compared with leptin receptor−deficient mice, in which ARC→PVH fibers are reduced [59,60].

The method used to study the fibers in the PVH is based on the quantification of the fluorescent signal, and it allows assessing the density of the fibers (estimated as the total area with specific fluorescent signal in the PVH) and their strength (estimated as the amount of fluorescent signal per area unit). As described in the Materials and Methods section, the method was simple to use, quantitative, and highly sensitive. The fact that similar results were obtained using

different experimental strategies reinforces the validity of the approach. The observation that the strength of the ARC$^{AgRP/NPY}$→PVH fibers increases in fasted mice is presumably due to an increase in the biosynthesis of the orexigenic peptides. The neurobiological bases underlying the fasting-induced increase of the density of the ARC$^{AgRP/NPY}$→PVH fibers are uncertain but may be due to an increase in the axonal arborization of these projections. Further studies are required to gain insights about the structural changes that determine the remodeling of the ARC$^{AgRP/NPY}$→PVH projections under fasting.

Activation of ARC$^{AgRP/NPY}$ neurons potently increases food intake and is essential for animals to cope with energy-deficit conditions [61−64]. Notably, the selective activation of ARC$^{AgRP/NPY}$→PVH projections evokes feeding, and the pharmacological blockade of ARC$^{AgRP/NPY}$→PVH projections reduces food intake induced by activation of ARC$^{AgRP/NPY}$ neurons [7,8,65,66]. In contrast, the activation of ARC$^{AgRP/NPY}$ neurons can acutely evoke feeding independently on the inhibition of ARC^{POMC} neurons [61]. Thus, the ARC$^{AgRP/NPY}$→PVH projections play a major role in the mediation of orexigenic effects of ARC$^{AgRP/NPY}$ neurons. Importantly, the activation of ARC$^{AgRP/NPY}$→PVH projections inhibits PVH neurons that control food intake, which in turn are known to inhibit food intake [7]. Indeed, acute chemogenetic inhibition of Single-minded1-expressing PVH neurons increases food intake [7,67], while its activation reduces food intake [68]. Strikingly, we found that the number c-Fos+ cells increases in the PVH of fasted mice, as has
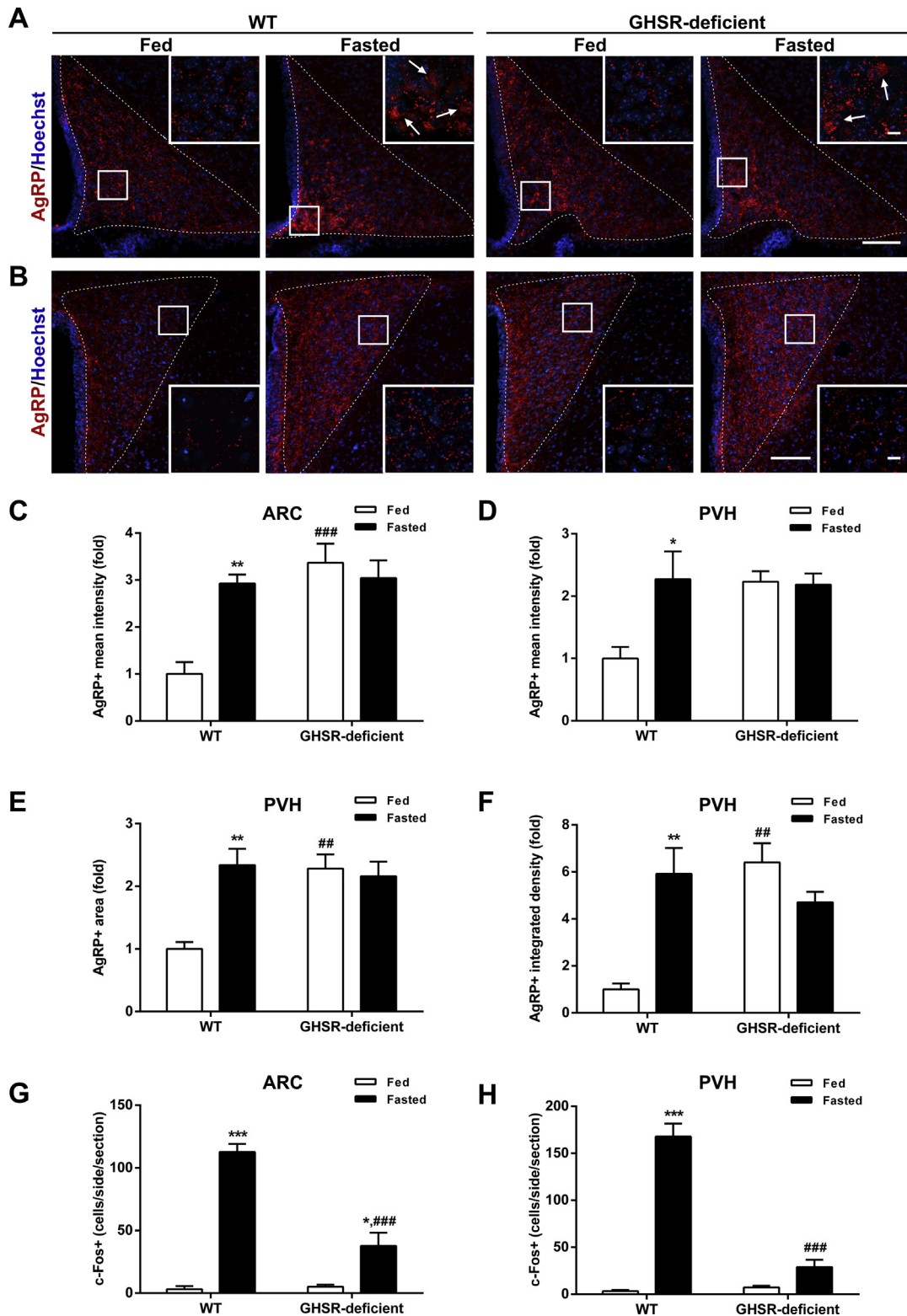
Figure 6: *Fasting-induced increase in ARC^{AgRP/NPY} → PVH projections is impaired in GHSR-deficient mice.* **(A, B)** Representative photomicrographs of the ARC and PVH coronal sections, respectively, of WT and GHSR-deficient mice in each experimental group, subjected to immunofluorescence against AgRP (red). Insets in each image depict high magnification images of the areas marked in low magnification images. Arrows point at AgRP-positive cells. Scale bars: 100 μm (low magnification) and 10 μm (high magnification). Cell nuclei labeled with Hoechst (blue). **(C)** Bar graph displaying the quantitative analysis of the mean fluorescence intensity of the AgRP-positive signal in the ARC of each experimental group (n = 4−5). **(D−F)** Bar graphs displaying the quantitative analysis of the mean fluorescence intensity, fluorescent area and integrated density of the AgRP-positive signal in the PVH of each experimental group (n = 4−5). **(G, H)** Bar graphs displaying the quantitative analysis of the number of c-Fos-positive cells in the ARC and PVH, respectively, of each experimental group (n = 7−11). Data represent the mean ± SEM and were compared by two-way ANOVA. *$p < 0.05$, **$p < 0.01$ and ***$p < 0.001$ vs. different condition, same genotype; ##$p < 0.01$ and ###$p < 0.001$ vs. same condition, different genotype.
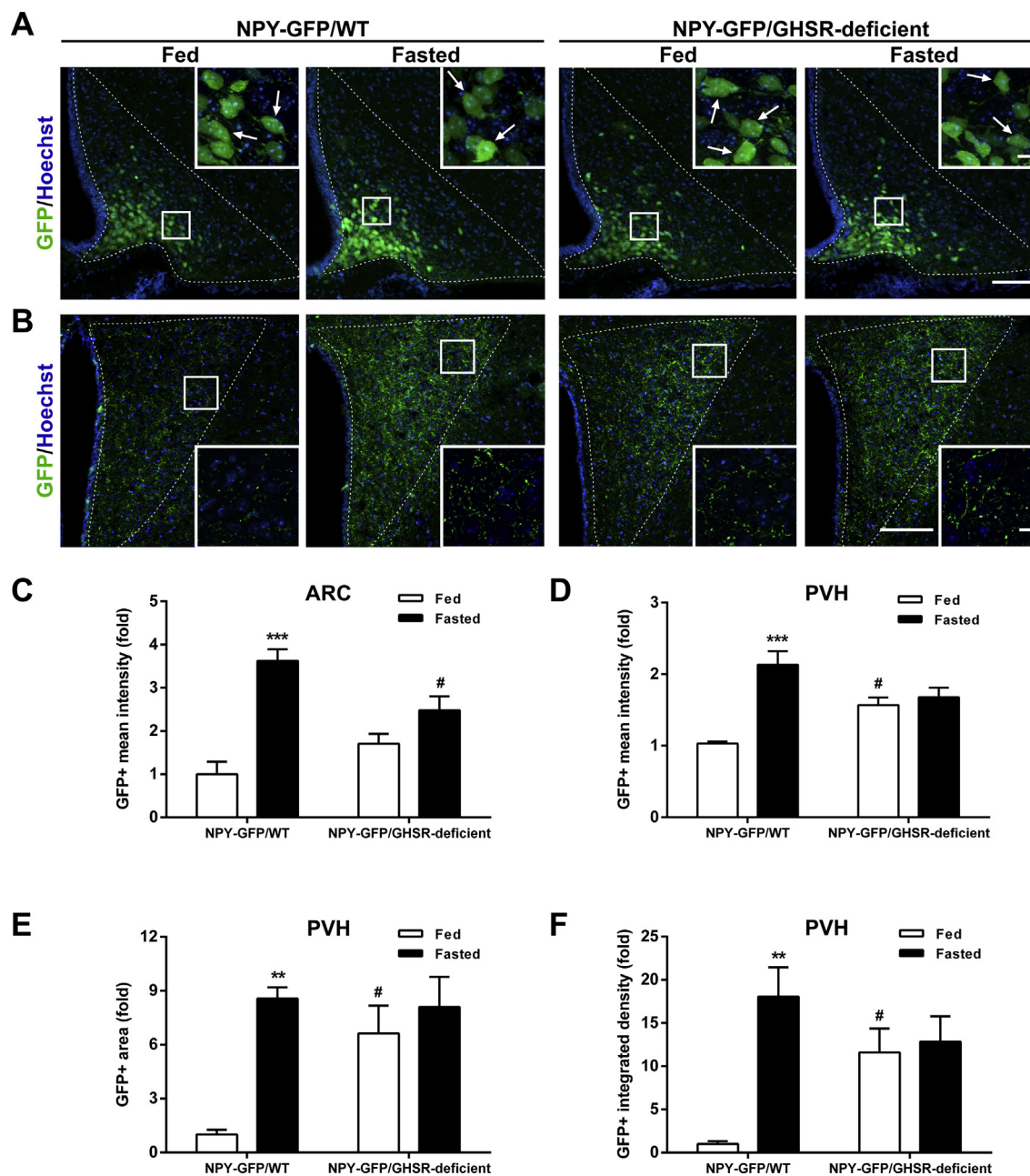
Figure 7: *Fasting-induced increase in ARC^NPY → PVH projections is impaired in NPY-GFP/GHSR-deficient mice.* **(A, B)** Representative photomicrographs of the ARC and PVH coronal sections, respectively, of NPY-GFP/WT and NPY-GFP/GHSR-deficient mice in each experimental group. Insets in each image depict high magnification images of the areas marked in low magnification images. Arrows point at GFP-positive cells. Scale bars: 100 μm (low magnification) and 10 μm (high magnification). Cell nuclei labeled with Hoechst (blue). **(C)** Bar graph displaying the quantitative analysis of the mean fluorescence intensity of the GFP-positive signal in the ARC of each experimental group (n = 5−6). **(D−F)** Bar graphs displaying the quantitative analysis of the mean fluorescence intensity, fluorescent area and integrated density of the GFP-positive signal in the PVH of each experimental group (n = 5−6). Data represent the mean ± SEM and were compared by two-way ANOVA. **$p < 0.01$ and ***$p < 0.001$ vs. different condition, same genotype; #$p < 0.05$ vs. same condition, different genotype.

been previously reported [69−71]. Fasting-induced PVH activation is not observed in ARC-ablated mice. Thus, ARC^AgRP/NPY→PVH projections seem to activate PVH neurons that are presumably not involved in food intake regulation. Establishing the identity of the PVH neurons activated by the ARC^AgRP/NPY→PVH projections in fasting conditions is essential to clarify the metabolic consequences of current observations. ARC^AgRP/NPY→PVH projections also target PVH neurons involved in the regulation of autonomic or neuroendocrine functions.

For instance, ARC^AgRP/NPY neurons activate the corticotrophin-releasing factor (CRF)−producing neurons of the PVH that regulate the activity of the hypothalamic-pituitary-adrenal axis, which in turn is upregulated under fasting in order to increase glycemia [72−74]. Thus, it can be hypothesized that the fasting-induced remodeling of the ARC^AgRP/NPY→PVH projections promotes activation of CRF neurons and further increases glucocorticoid levels, which would protect fasted mice from severe hypoglycemia.
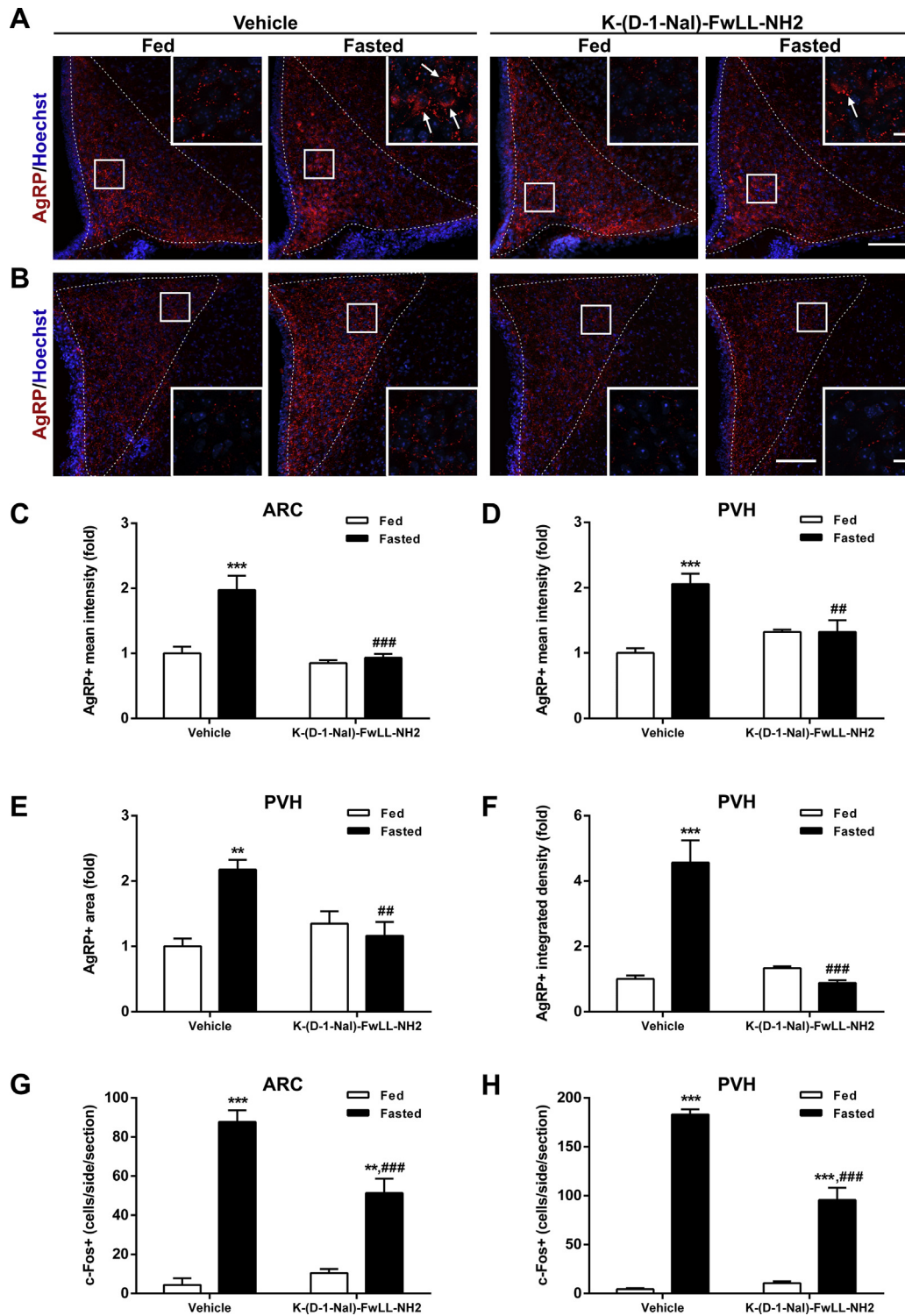
Figure 8: *Fasting-induced increase of ARC$^{AgRP/NPY}$→ PVH projections is impaired in WT mice centrally treated with the GHSR blocker K-(D-1-Nal)-FwLL-NH$_2$.* **(A, B)** Representative photomicrographs of the ARC and PVH coronal sections, respectively, of WT mice ICV-treated with vehicle or with the GHSR blocker K-(D-1-Nal)-FwLL-NH2 in each experimental group, subjected to immunofluorescence against AgRP (red). Insets in each image depict high magnification images of the areas marked in low magnification images. Arrows point at AgRP-positive cells. Scale bars: 100 μm (low magnification) and 10 μm (high magnification). Cell nuclei labeled with Hoechst (blue). **(C)** Bar graph displaying the quantitative analysis of the mean fluorescence intensity of the AgRP-positive signal in the ARC of each experimental group (n = 4). **(D−F)** Bar graphs displaying the quantitative analysis of the mean fluorescence intensity, fluorescent area and integrated density of the AgRP-positive signal in the PVH of each experimental group (n = 4). **(G, H)** Bar graphs displaying the quantitative analysis of the number of c-Fos-positive cells in the ARC and PVH, respectively, of each experimental group (n = 4−7). Data represent the mean ± SEM and were compared by two-way ANOVA. **p < 0.01 and ***p < 0.001 vs. different condition, same treatment; ##p < 0.01 and ###p < 0.001 vs. same condition, different treatment.

ARC^{AgRP/NPY} neurons express the highest levels of GHSR within the brain [18,22,75], and they are located in the ventromedial region of the ARC, near fenestrated capillaries, to sense plasma ghrelin [20,76—78]. ARC^{AgRP/NPY} neurons are strongly activated by ghrelin, and they mediate the orexigenic effects of the circulating hormone [18,79—81]. Previous evidence has shown that ghrelin stimulates neuronal plasticity [82]. In particular, ghrelin treatment in mice increases excitatory inputs onto ARC^{AgRP/NPY} neurons [31,44]. Also, ghrelin stimulates spine reorganization in hippocampal slice cultures [83], promotes the formation of hippocampal dendritic spine synapses, and facilitates long-term potentiation in vivo [84]. *In vitro*, ghrelin stimulates synapse formation of hippocampal neurons [85] and neurite outgrowth in dopamine neurons of the ARC [86]. We show here that fasting-induced morphological remodeling of the ARC^{AgRP/NPY}→PVH projections and PVH activation require GHSR signaling. Of note, GHSR signals via ghrelin-dependent and ghrelin-independent (or constitutive) modes, and both modalities of GHSR signaling are upregulated in fasting states, when plasma ghrelin and hypothalamic GHSR levels increase [30,87]. Here, both modes of GHSR activity were abrogated in GHSR-deficient mice as well as in K-(D-1-Nal)-FwLL-NH₂—treated mice because this compound blocks ghrelin-evoked and constitutive GHSR activities [30,39]. Thus, current results do not allow us to discriminate whether the different modalities of GHSR activity play a distinctive role on the remodeling of the ARC^{AgRP/NPY}→PVH projections.

The early nutritional and endocrine environment causes effects on the ARC projections that remain during adulthood [88—90]. In this regard, a previous study showed that the pharmacological blockage of ghrelin during the preweaning period increases the density of the ARC^{AgRP/NPY}→PVH fibers in the adult mouse brain and that ghrelin knockout mice show a higher density of ARC^{AgRP/NPY}→PVH fibers in the preweaning period, which then normalizes during adulthood [91]. The referenced study also showed that ghrelin does not affect the density of ARC^{AgRP/NPY}→PVH fibers in the adult brain, suggesting that ghrelin-evoked GHSR signaling alone is not sufficient to mediate such effects [91]. In line with the notion that ghrelin inhibits the development of ARC^{AgRP/NPY}→PVH projections during early postnatal life, we found that adult GHSR-deficient mice displayed a higher density of ARC^{AgRP/NPY}→PVH fibers in the ad libitum fed condition. Thus, it seems that GHSR signaling inhibits the development of ARC→PVH neuronal projections in the preweaning stages and then is required for the fasting-induced increase of the density of ARC^{AgRP/NPY}→PVH fibers in adulthood. The neurobiology underlying these apparently divergent effects remains uncertain. Notably, ARC^{AgRP/NPY} neurons are stimulated by leptin during the preweaning period and inhibited in the adulthood stages, and this developmental switch has been attributed to the parallel acquisition of the functional K_{ATP} channels [92]. In addition, chemotrophic factors regulating axonal growth are developmentally regulated, and recent evidence has highlighted their role as early regulators of the connectivity of the hypothalamic circuits controlling food intake [90,93]. The potential role of these chemotrophic factors in controlling the remodeling of hypothalamic projections during adulthood remains unknown.

Finally, it is important to stress that we investigated the remodeling of the ARC→PVH projections and the implications of GHSR activity in 48-h fasted mice because previous studies have highlighted the fact that severe energy-deficit conditions are required to uncover some essential roles of ghrelin [15]. Such experimental conditions may have favored our ability to detect remodeling of the ARC^{AgRP/NPY}→PVH projections, since changes in axon structure require some time to take place [94]. Interestingly, a recent study using diffusion-tensor imaging combined with a probabilistic tractography algorithm suggested that the connectivity is altered in the hypothalamus of patients with anorexia nervosa [95]. Thus, current observations may help to model the hypothalamic adaptations that occur in response to chronic conditions with extreme energy deficit, such as cachexia, anorexia, and malnutrition.

5. CONCLUSIONS

Overall, we provide neuroanatomical and functional evidence indicating that the ARC^{AgRP/NPY}→PVH projections undergo major morphological remodeling under fasting and that GHSR signaling is required for these effects. These findings highlight the fact that connectivity between hypothalamic circuits regulating food intake is highly plastic in the adult brain and reveal a novel role for ghrelin.

CONFLICTS OF INTEREST

Agustina Cabral, Ph.D., Gimena Fernandez, Ph.D., María J. Tolosa, Ph.D., Ángeles Rey-Moggia, B.S., Gastón Calfa, Ph.D., Pablo N. De Francesco, Ph.D., and Mario Perello, Ph.D., declare that the research was conducted in the absence of any commercial or financial relationships that could be construed as a potential conflict of interest.

APPENDIX A. SUPPLEMENTARY DATA

Supplementary data to this article can be found online at https://doi.org/10.1016/j.molmet.2019.11.014.

REFERENCES

[1] Garcia-Segura, L.M., 2009. Hormones and brain plasticity. Oxford ; New York: Oxford University Press.

[2] Oliet, S.H., 2002. Functional consequences of morphological neuroglial changes in the magnocellular nuclei of the hypothalamus. Journal of Neuroendocrinology 14(3):241—246.

[3] Prevot, V., 2002. Glial-neuronal-endothelial interactions are involved in the control of GnRH secretion. Journal of Neuroendocrinology 14(3):247—255.

[4] Ebling, F.J., Barrett, P., 2008. The regulation of seasonal changes in food intake and body weight. Journal of Neuroendocrinology 20(6):827—833.

[5] Zeltser, L.M., Seeley, R.J., Tschop, M.H., 2012. Synaptic plasticity in neuronal circuits regulating energy balance. Nature Neuroscience 15(10):1336—1342.

[6] Sohn, J.W., 2015. Network of hypothalamic neurons that control appetite. BMB Reports 48(4):229—233.

[7] Atasoy, D., Betley, J.N., Su, H.H., Sternson, S.M., 2012. Deconstruction of a neural circuit for hunger. Nature 488(7410):172—177.

[8] Betley, J.N., Cao, Z.F., Ritola, K.D., Sternson, S.M., 2013. Parallel, redundant circuit organization for homeostatic control of feeding behavior. Cell 155(6):1337—1350.

Original Article

[9] Chen, Y., Lin, Y.C., Kuo, T.W., Knight, Z.A., 2015. Sensory detection of food rapidly modulates arcuate feeding circuits. Cell 160(5):829—841.

[10] Krashes, M.J., Shah, B.P., Madara, J.C., Olson, D.P., Strochlic, D.E., Garfield, A.S., et al., 2014. An excitatory paraventricular nucleus to AgRP neuron circuit that drives hunger. Nature 507(7491):238—242.

[11] Henry, F.E., Sugino, K., Tozer, A., Branco, T., Sternson, S.M., 2015. Cell type-specific transcriptomics of hypothalamic energy-sensing neuron responses to weight-loss. Elife 4.

[12] Liu, T., Kong, D., Shah, B.P., Ye, C., Koda, S., Saunders, A., et al., 2012. Fasting activation of AgRP neurons requires NMDA receptors and involves spinogenesis and increased excitatory tone. Neuron 73(3):511—522.

[13] Kojima, M., Hosoda, H., Date, Y., Nakazato, M., Matsuo, H., Kangawa, K., 1999. Ghrelin is a growth-hormone-releasing acylated peptide from stomach. Nature 402(6762):656—660.

[14] Muller, T.D., Nogueiras, R., Andermann, M.L., Andrews, Z.B., Anker, S.D., Argente, J., et al., 2015. Ghrelin. Mol Metab 4(6):437—460.

[15] Goldstein, J.L., Zhao, T.J., Li, R.L., Sherbet, D.P., Liang, G., Brown, M.S., 2011. Surviving starvation: essential role of the ghrelin-growth hormone axis. Cold Spring Harbor Symposia on Quantitative Biology 76:121—127.

[16] Perello, M., Dickson, S.L., 2015. Ghrelin signalling on food reward: a salient link between the gut and the mesolimbic system. Journal of Neuroendocrinology 27(6):424—434.

[17] Zhao, T.J., Liang, G., Li, R.L., Xie, X., Sleeman, M.W., Murphy, A.J., et al., 2010. Ghrelin O-acyltransferase (GOAT) is essential for growth hormone-mediated survival of calorie-restricted mice. Proceedings of the National Academy of Sciences of the United States of America 107(16):7467—7472.

[18] Wang, Q., Liu, C., Uchida, A., Chuang, J.C., Walker, A., Liu, T., et al., 2014. Arcuate AgRP neurons mediate orexigenic and glucoregulatory actions of ghrelin. Molecular Metabolism 3(1):64—72.

[19] Howard, A.D., Feighner, S.D., Cully, D.F., Arena, J.P., Liberator, P.A., Rosenblum, C.I., et al., 1996. A receptor in pituitary and hypothalamus that functions in growth hormone release. Science 273(5277):974—977.

[20] Cabral, A., Valdivia, S., Fernandez, G., Reynaldo, M., Perello, M., 2014. Divergent neuronal circuitries underlying acute orexigenic effects of peripheral or central ghrelin: critical role of brain accessibility. Journal of Neuroendocrinology 26(8):542—554.

[21] Luquet, S., Phillips, C.T., Palmiter, R.D., 2007. NPY/AgRP neurons are not essential for feeding responses to glucoprivation. Peptides 28(2):214—225.

[22] Campbell, J.N., Macosko, E.Z., Fenselau, H., Pers, T.H., Lyubetskaya, A., Tenen, D., et al., 2017. A molecular census of arcuate hypothalamus and median eminence cell types. Nature Neuroscience 20(3):484—496.

[23] Perello, M., Scott, M.M., Sakata, I., Lee, C.E., Chuang, J.C., Osborne-Lawrence, S., et al., 2012. Functional implications of limited leptin receptor and ghrelin receptor coexpression in the brain. Journal of Comparative Neurology 520(2):281—294.

[24] Dickson, S.L., Luckman, S.M., 1997. Induction of c-fos messenger ribonucleic acid in neuropeptide Y and growth hormone (GH)-releasing factor neurons in the rat arcuate nucleus following systemic injection of the GH secretagogue, GH-releasing peptide-6. Endocrinology 138(2):771—777.

[25] Bewick, G.A., Gardiner, J.V., Dhillo, W.S., Kent, A.S., White, N.E., Webster, Z., et al., 2005. Post-embryonic ablation of AgRP neurons in mice leads to a lean, hypophagic phenotype. The FASEB Journal 19(12):1680—1682.

[26] Yasrebi, A., Hsieh, A., Mamounis, K.J., Krumm, E.A., Yang, J.A., Magby, J., et al., 2016. Differential gene regulation of GHSR signaling pathway in the arcuate nucleus and NPY neurons by fasting, diet-induced obesity, and 17beta-estradiol. Molecular and Cellular Endocrinology 422:42—56.

[27] Luckman, S.M., Rosenzweig, I., Dickson, S.L., 1999. Activation of arcuate nucleus neurons by systemic administration of leptin and growth hormone-releasing peptide-6 in normal and fasted rats. Neuroendocrinology 70(2):93—100.

[28] Cabral, A., Cornejo, M.P., Fernandez, G., De Francesco, P.N., Garcia-Romero, G., Uriarte, M., et al., 2017. Circulating ghrelin acts on GABA neurons of the area postrema and mediates gastric emptying in male mice. Endocrinology 158(5):1436—1449.

[29] Luque, R.M., Park, S., Kineman, R.D., 2007. Severity of the catabolic condition differentially modulates hypothalamic expression of growth hormone-releasing hormone in the fasted mouse: potential role of neuropeptide Y and corticotropin-releasing hormone. Endocrinology 148(1):300—309.

[30] Fernandez, G., Cabral, A., Andreoli, M.F., Labarthe, A., M'Kadmi, C., Ramos, J.G., et al., 2018. Evidence supporting a role for constitutive ghrelin receptor signaling in fasting-induced hyperphagia in male mice. Endocrinology 159(2):1021—1034.

[31] Yang, Y., Atasoy, D., Su, H.H., Sternson, S.M., 2011. Hunger states switch a flip-flop memory circuit via a synaptic AMPK-dependent positive feedback loop. Cell 146(6):992—1003.

[32] van den Pol, A.N., Yao, Y., Fu, L.Y., Foo, K., Huang, H., Coppari, R., et al., 2009. Neuromedin B and gastrin-releasing peptide excite arcuate nucleus neuropeptide Y neurons in a novel transgenic mouse expressing strong Renilla green fluorescent protein in NPY neurons. Journal of Neuroscience 29(14):4622—4639.

[33] Zigman, J.M., Nakano, Y., Coppari, R., Balthasar, N., Marcus, J.N., Lee, C.E., et al., 2005. Mice lacking ghrelin receptors resist the development of diet-induced obesity. Journal of Clinical Investigation 115(12):3564—3572.

[34] National Research Council (U.S.). Committee for the update of the guide for the Care and use of laboratory animals., Institute for laboratory animal research (U.S.), national academies press (U.S.), 2011. Guide for the care and use of laboratory animals, 8th ed. Washington, D.C: National Academies Press.

[35] Pozzo-Miller, L.D., Inoue, T., Murphy, D.D., 1999. Estradiol increases spine density and NMDA-dependent Ca2+ transients in spines of CA1 pyramidal neurons from hippocampal slices. Journal of Neurophysiology 81(3):1404—1411.

[36] Giachero, M., Calfa, G.D., Molina, V.A., 2013. Hippocampal structural plasticity accompanies the resulting contextual fear memory following stress and fear conditioning. Learning & Memory 20(11):611—616.

[37] Bender, C.L., Giachero, M., Comas-Mutis, R., Molina, V.A., Calfa, G.D., 2018. Stress influences the dynamics of hippocampal structural remodeling associated with fear memory extinction. Neurobiology of Learning and Memory 155:412—421.

[38] Fernandez, G., Cabral, A., Cornejo, M.P., De Francesco, P.N., Garcia-Romero, G., Reynaldo, M., et al., 2016. Des-acyl ghrelin directly targets the arcuate nucleus in a ghrelin-receptor independent manner and impairs the orexigenic effect of ghrelin. Journal of Neuroendocrinology 28(2):12349.

[39] Els, S., Schild, E., Petersen, P.S., Kilian, T.M., Mokrosinski, J., Frimurer, T.M., et al., 2012. An aromatic region to induce a switch between agonism and inverse agonism at the ghrelin receptor. Journal of Medicinal Chemistry 55(17):7437—7449.

[40] Cabral, A., Suescun, O., Zigman, J.M., Perello, M., 2012. Ghrelin indirectly activates hypophysiotropic CRF neurons in rodents. PLoS One 7(2):e31462.

[41] Schindelin, J., Arganda-Carreras, I., Frise, E., Kaynig, V., Longair, M., Pietzsch, T., et al., 2012. Fiji: an open-source platform for biological-image analysis. Nature Methods 9(7):676—682.

[42] Paxinos, G., Franklin, K.B.J., 2001. The mouse brain in stereotaxic coordinates, vol. 2. San Diego: Academic Press.

[43] Abercrombie, M., 1946. Estimation of nuclear population from microtome sections. The Anatomical Record 94:239—247.

[44] Pinto, S., Roseberry, A.G., Liu, H., Diano, S., Shanabrough, M., Cai, X., et al., 2004. Rapid rewiring of arcuate nucleus feeding circuits by leptin. Science 304(5667):110—115.

[45] Takahashi, K.A., Cone, R.D., 2005. Fasting induces a large, leptin-dependent increase in the intrinsic action potential frequency of orexigenic arcuate nucleus neuropeptide Y/Agouti-related protein neurons. Endocrinology 146(3): 1043—1047.

[46] Perello, M., Stuart, R.C., Nillni, E.A., 2007. Differential effects of fasting and leptin on proopiomelanocortin peptides in the arcuate nucleus and in the nucleus of the solitary tract. American Journal of Physiology. Endocrinology and Metabolism 292(5):E1348—E1357.

[47] van den Top, M., Lee, K., Whyment, A.D., Blanks, A.M., Spanswick, D., 2004. Orexigen-sensitive NPY/AgRP pacemaker neurons in the hypothalamic arcuate nucleus. Nature Neuroscience 7(5):493—494.

[48] Cowley, M.A., Smart, J.L., Rubinstein, M., Cerdan, M.G., Diano, S., Horvath, T.L., et al., 2001. Leptin activates anorexigenic POMC neurons through a neural network in the arcuate nucleus. Nature 411(6836):480—484.

[49] Roseberry, A.G., Liu, H., Jackson, A.C., Cai, X., Friedman, J.M., 2004. Neuropeptide Y-mediated inhibition of proopiomelanocortin neurons in the arcuate nucleus shows enhanced desensitization in ob/ob mice. Neuron 41(5):711—722.

[50] Bains, J.S., Wamsteeker Cusulin, J.I., Inoue, W., 2015. Stress-related synaptic plasticity in the hypothalamus. Nature Reviews Neuroscience 16(7):377—388.

[51] Sawchenko, P.E., 1998. Toward a new neurobiology of energy balance, appetite, and obesity: the anatomists weigh in. Journal of Comparative Neurology 402(4):435—441.

[52] Watts, A.G., 2005. Glucocorticoid regulation of peptide genes in neuroendocrine CRH neurons: a complexity beyond negative feedback. Frontiers in Neuroendocrinology 26(3—4):109—130.

[53] Broberger, C., De Lecea, L., Sutcliffe, J.G., Hokfelt, T., 1998. Hypocretin/orexin- and melanin-concentrating hormone-expressing cells form distinct populations in the rodent lateral hypothalamus: relationship to the neuropeptide Y and agouti gene-related protein systems. Journal of Comparative Neurology 402(4):460—474.

[54] Hahn, T.M., Breininger, J.F., Baskin, D.G., Schwartz, M.W., 1998. Coexpression of Agrp and NPY in fasting-activated hypothalamic neurons. Nature Neuroscience 1(4):271—272.

[55] Legradi, G., Lechan, R.M., 1998. The arcuate nucleus is the major source for neuropeptide Y-innervation of thyrotropin-releasing hormone neurons in the hypothalamic paraventricular nucleus. Endocrinology 139(7):3262—3270.

[56] Cyr, N.E., Toorie, A.M., Steger, J.S., Sochat, M.M., Hyner, S., Perello, M., et al., 2013. Mechanisms by which the orexin NPY regulates anorexigenic alpha-MSH and TRH. American Journal of Physiology. Endocrinology and Metabolism 304(6):E640—E650.

[57] Breen, T.L., Conwell, I.M., Wardlaw, S.L., 2005. Effects of fasting, leptin, and insulin on AGRP and POMC peptide release in the hypothalamus. Brain Research 1032(1—2):141—148.

[58] Pritchard, L.E., Oliver, R.L., McLoughlin, J.D., Birtles, S., Lawrence, C.B., Turnbull, A.V., et al., 2003. Proopiomelanocortin-derived peptides in rat cerebrospinal fluid and hypothalamic extracts: evidence that secretion is regulated with respect to energy balance. Endocrinology 144(3):760—766.

[59] Ramos-Lobo, A.M., Teixeira, P.D., Furigo, I.C., Melo, H.M., de, M.L.E.S.N., De Felice, F.G., et al., 2019. Long-term consequences of the absence of leptin signaling in early life. Elife 8.

[60] Bouret, S.G., Draper, S.J., Simerly, R.B., 2004. Formation of projection pathways from the arcuate nucleus of the hypothalamus to hypothalamic regions implicated in the neural control of feeding behavior in mice. Journal of Neuroscience 24(11):2797—2805.

[61] Aponte, Y., Atasoy, D., Sternson, S.M., 2011. AGRP neurons are sufficient to orchestrate feeding behavior rapidly and without training. Nature Neuroscience 14(3):351—355.

[62] Krashes, M.J., Koda, S., Ye, C., Rogan, S.C., Adams, A.C., Cusher, D.S., et al., 2011. Rapid, reversible activation of AgRP neurons drives feeding behavior in mice. Journal of Clinical Investigation 121(4):1424—1428.

[63] Luquet, S., Perez, F.A., Hnasko, T.S., Palmiter, R.D., 2005. NPY/AgRP neurons are essential for feeding in adult mice but can be ablated in neonates. Science 310(5748):683—685.

[64] Wu, C.S., Bongmba, O.Y.N., Lee, J.H., Tuchaai, E., Zhou, Y., Li, D.P., et al., 2019. Ghrelin receptor in agouti-related peptide neurones regulates metabolic adaptation to calorie restriction. Journal of Neuroendocrinology 31(7):e12763.

[65] Chen, Y., Lin, Y.C., Zimmerman, C.A., Essner, R.A., Knight, Z.A., 2016. Hunger neurons drive feeding through a sustained, positive reinforcement signal. Elife 5.

[66] Padilla, S.L., Qiu, J., Soden, M.E., Sanz, E., Nestor, C.C., Barker, F.D., et al., 2016. Agouti-related peptide neural circuits mediate adaptive behaviors in the starved state. Nature Neuroscience 19(5):734—741.

[67] Vardy, E., Robinson, J.E., Li, C., Olsen, R.H.J., DiBerto, J.F., Giguere, P.M., et al., 2015. A new DREADD facilitates the multiplexed chemogenetic interrogation of behavior. Neuron 86(4):936—946.

[68] Sutton, A.K., Pei, H., Burnett, K.H., Myers Jr., M.G., Rhodes, C.J., Olson, D.P., 2014. Control of food intake and energy expenditure by Nos1 neurons of the paraventricular hypothalamus. Journal of Neuroscience 34(46):15306—15318.

[69] Miller, I., Ronnett, G.V., Moran, T.H., Aja, S., 2004. Anorexigenic C75 alters c-Fos in mouse hypothalamic and hindbrain subnuclei. NeuroReport 15(5):925—929.

[70] Morikawa, Y., Ueyama, E., Senba, E., 2004. Fasting-induced activation of mitogen-activated protein kinases (ERK/p38) in the mouse hypothalamus. Journal of Neuroendocrinology 16(2):105—112.

[71] Okamoto, S., Sato, T., Tateyama, M., Kageyama, H., Maejima, Y., Nakata, M., et al., 2018. Activation of AMPK-regulated CRH neurons in the PVH is sufficient and necessary to induce dietary preference for carbohydrate over fat. Cell Reports 22(3):706—721.

[72] Li, C., Chen, P., Smith, M.S., 2000. Corticotropin releasing hormone neurons in the paraventricular nucleus are direct targets for neuropeptide Y neurons in the arcuate nucleus: an anterograde tracing study. Brain Research 854(1—2): 122—129.

[73] Dimitrov, E.L., DeJoseph, M.R., Brownfield, M.S., Urban, J.H., 2007. Involvement of neuropeptide Y Y1 receptors in the regulation of neuroendocrine corticotropin-releasing hormone neuronal activity. Endocrinology 148(8): 3666—3673.

[74] Sarkar, S., Lechan, R.M., 2003. Central administration of neuropeptide Y reduces alpha-melanocyte-stimulating hormone-induced cyclic adenosine 5'-monophosphate response element binding protein (CREB) phosphorylation in pro-thyrotropin-releasing hormone neurons and increases CREB phosphorylation in corticotropin-releasing hormone neurons in the hypothalamic paraventricular nucleus. Endocrinology 144(1):281—291.

[75] Willesen, M.G., Kristensen, P., Romer, J., 1999. Co-localization of growth hormone secretagogue receptor and NPY mRNA in the arcuate nucleus of the rat. Neuroendocrinology 70(5):306—316.

[76] Schaeffer, M., Langlet, F., Lafont, C., Molino, F., Hodson, D.J., Roux, T., et al., 2013. Rapid sensing of circulating ghrelin by hypothalamic appetite-modifying neurons. Proceedings of the National Academy of Sciences of the United States of America 110(4):1512—1517.

[77] Ciofi, P., Garret, M., Lapirot, O., Lafon, P., Loyens, A., Prevot, V., et al., 2009. Brain-endocrine interactions: a microvascular route in the mediobasal hypothalamus. Endocrinology 150(12):5509—5519.

[78] Perello, M., Cabral, A., Cornejo, M.P., De Francesco, P.N., Fernandez, G., Uriarte, M., 2019. Brain accessibility delineates the central effects of circulating ghrelin. Journal of Neuroendocrinology 31(7):e12677.

[79] Nakazato, M., Murakami, N., Date, Y., Kojima, M., Matsuo, H., Kangawa, K., et al., 2001. A role for ghrelin in the central regulation of feeding. Nature 409(6817):194—198.

[80] Cowley, M.A., Smith, R.G., Diano, S., Tschop, M., Pronchuk, N., Grove, K.L., et al., 2003. The distribution and mechanism of action of ghrelin in the CNS

demonstrates a novel hypothalamic circuit regulating energy homeostasis. Neuron 37(4):649—661.

[81] Chen, S.R., Chen, H., Zhou, J.J., Pradhan, G., Sun, Y., Pan, H.L., et al., 2017. Ghrelin receptors mediate ghrelin-induced excitation of agouti-related protein/ neuropeptide Y but not pro-opiomelanocortin neurons. Journal of Neuro-chemistry 142(4):512—520.

[82] Serrenho, D., Santos, S.D., Carvalho, A.L., 2019. The role of ghrelin in regulating synaptic function and plasticity of feeding-associated circuits. Frontiers in Cellular Neuroscience 13:205.

[83] Berrout, L., Isokawa, M., 2012. Ghrelin promotes reorganization of dendritic spines in cultured rat hippocampal slices. Neuroscience Letters 516(2):280—284.

[84] Diano, S., Farr, S.A., Benoit, S.C., McNay, E.C., da Silva, I., Horvath, B., et al., 2006. Ghrelin controls hippocampal spine synapse density and memory per-formance. Nature Neuroscience 9(3):381—388.

[85] Stoyanova II, , le Feber, J., 2014. Ghrelin accelerates synapse formation and activity development in cultured cortical networks. BMC Neuroscience 15:49.

[86] Huang, S., Lee, S.A., Oswald, K.E., Fry, M., 2015. Ghrelin alters neurite outgrowth and electrophysiological properties of mouse ventrolateral arcuate tyrosine hydroxylase neurons in culture. Biochemical and Biophysical Research Communications 466(4):682—688.

[87] Lopez Soto, E.J., Agosti, F., Cabral, A., Mustafa, E.R., Damonte, V.M., Gandini, M.A., et al., 2015. Constitutive and ghrelin-dependent GHSR1a activation impairs CaV2.1 and CaV2.2 currents in hypothalamic neurons. The Journal of General Physiology 146(3):205—219.

[88] Bouret, S.G., 2017. Development of hypothalamic circuits that control food intake and energy balance. In: Harris, R.B.S. (Ed.), Appetite and food intake: central control: Boca Raton (FL). p. 135—54.

[89] Caron, E., Ciofi, P., Prevot, V., Bouret, S.G., 2012. Alteration in neonatal nutrition causes perturbations in hypothalamic neural circuits controlling reproductive function. Journal of Neuroscience 32(33):11486—11494.

[90] Muscatelli, F., Bouret, S.G., 2018. Wired for eating: how is an active feeding circuitry established in the postnatal brain? Current Opinion in Neurobiology 52:165—171.

[91] Steculorum, S.M., Collden, G., Coupe, B., Croizier, S., Lockie, S., Andrews, Z.B., et al., 2015. Neonatal ghrelin programs development of hy-pothalamic feeding circuits. Journal of Clinical Investigation 125(2):846—858.

[92] Baquero, A.F., de Solis, A.J., Lindsley, S.R., Kirigiti, M.A., Smith, M.S., Cowley, M.A., et al., 2014. Developmental switch of leptin signaling in arcuate nucleus neurons. Journal of Neuroscience 34(30):9982—9994.

[93] van der Klaauw, A.A., Croizier, S., Mendes de Oliveira, E., Stadler, L.K.J., Park, S., Kong, Y., et al., 2019. Human semaphorin 3 variants link melano-cortin circuit development and energy balance. Cell 176(4):729—742 e718.

[94] Gibson, D.A., Ma, L., 2011. Developmental regulation of axon branching in the vertebrate nervous system. Development 138(2):183—195.

[95] Florent, V., Baroncini, M., Jissendi-Tchofo, P., Lopes, R., Vanhoutte, M., Rasika, S., et al., 2019. Hypothalamic structural and functional imbalances in anorexia nervosa. Neuroendocrinology. https://doi.org/10.1159/000503147 [Epub ahead of print].